4D variational data assimilation for locally nested models: optimality system and preliminary experiments

Laurent Debreu, Ehouarn Simon, Eric Blayo

INSTITUT NATIONAL DE RECHERCHE EN INFORMATIQUE ET EN AUTOMATIQUE

4D variational data assimilation for locally nested models: optimality system and preliminary numerical experiments

Laurent Debreu — Ehouarn Simon — Eric Blayo

N° 7675

July 2011

Observation and Modeling for Environmental Sciences

ISSN 0249-6399 ISRN INRIA/RR--7675--FR+ENG

INSTITUT NATIONAL
DE RECHERCHE
EN INFORMATIQUE
ET EN AUTOMATIQUE

INRIA

centre de recherche
GRENOBLE - RHÔNE-ALPES

4D variational data assimilation for locally nested models: optimality system and preliminary numerical experiments

Laurent Debreu* , Ehouarn Simon†, Eric Blayo‡

Theme : Observation and Modeling for Environmental Sciences
Équipe-Projet Moise

Rapport de recherche n° 7675 — July 2011 — 19 pages

Abstract: We address the problem of adapting the four dimensional variational data assimilation method to a numerical model which employs local mesh refinement to improve its solution. We are concerned with structured meshes where a high resolution grid is nested into a coarser resolution grid which covers the entire domain. The derivation of the adjoint of the resulting locally nested model is presented. Both continuous and discrete versions are given. The new algorithms are then successfully applied to a 1D shallow water model with control of the initial condition.

Key-words: Variational data assimilation methods, Local mesh refinement, Shallow Water, Ocean modelling

* INRIA and Jean Kuntzmann Laboratory, Laurent.Debreu@inria.fr
† Nansen Environmental and Remote Sensing Center, Bergen, Norway, ehouarn.simon@nersc.no
‡ Grenoble University and Jean Kuntzmann Laboratory, Eric.Blayo@imag.fr

Centre de recherche INRIA Grenoble – Rhône-Alpes
655, avenue de l'Europe, 38334 Montbonnot Saint Ismier
Téléphone : +33 4 76 61 52 00 — Télécopie +33 4 76 61 52 52

4D variational data assimilation for locally nested models: optimality system and preliminary numerical experiments

Résumé : La méthode variationnelle d'assimilation de données est adaptée au cas d'un modèle numérique qui effectue du raffinement local de maillage pour améliorer la solution. Nous regardons le cas des maillages structurés où une grille à haute résolution est emboitée dans une grille à basse résolution qui recouvre l'ensemble du domaine. La dérivation du modèle adjoint correspondant est présentée. A la fois les formulations continues et discrètes sont données. Ces nouveaux algorithmes sont ensuite testés sur un modèle en eau peu profonde avec comme variable de contrôle la condition initiale.

Mots-clés : Assimilation variationnelle de données, Raffinement local de maillage, Shallow Water, modélisation océanique

1 INTRODUCTION

One of the main advantages of unstructured meshes over structured meshes is the ability to refine the grid in areas of interest. However, in some areas of applications like atmosphere or ocean modelling, structured grids remain the favorite choice due to their lower computational cost and their respect of basic physical properties like local conservation or monotonicity (even if to these respects, use of discontinuous Galerkin methods on unstructured meshes solve several problems [1]). Therefore variational data assimilation methods, which try to combine efficiently model, observations and error statistics, have been integrated for a while in ocean or atmosphere models based on structured meshes. They are now used operationally in several numerical weather or ocean prediction centers. However, when local mesh refinement is applied, the applications of data assimilation are more advanced in models based on unstructured meshes (e.g. [2]) since the refinement is more naturally handled.

Local mesh refinement methods for structured meshes, sometimes called *nesting* or *embedding* methods, are now widely used. Their general idea is to increase locally the resolution of the mesh (to make a zoom) in areas where it seems to be necessary, either to improve the solution specifically in the area of the zoom or to improve more globally the quality of the solution. For that purpose, the same model is run on the different grids of a hierarchy. A distinction is made between "one-way" algorithms, where a coarse grid solution is used to provide boundary conditions to a local high resolution grid and the "two way" case where there is also a feedback from the fine to the coarse grid. These methods have been used for a while in atmosphere and ocean modelling and are presented in several papers (e.g. [3, 4, 5, 6, 7, 8]). In a more complex approach, the refinement can also be made adaptive in time with some periodic reconstruction of the grid hierarchy following a refinement criterion (see [9]). Readers can find applications of adaptive mesh refinement to atmosphere modeling in [10] and to ocean modeling in [11, 12, 13].

A natural question is how to apply data assimilation methods to numerical models which employ local mesh refinement to improve their solution ? The main question is here how to properly take into account grid interactions in the assimilation process, both in the case of one-way and two-way algorithms. This is the subject of the present paper. Another question, which is of particular importance for realistic experiments, is how to consistently define multiresolution error covariance matrices. This point is discussed in [14].

In this paper, we focus on variational data assimilation methods based on optimal control theory. In several papers, a quite different problem has been addressed: the coupling between mesh refinement methods and optimization problems to solve the optimization problem via a multigrid algorithm. The most popular approach is the "one shot" method [15]. In a "one shot" method, the optimization problem on a high resolution grid is accelerated by solving the optimization problem on a coarser resolution grid covering the same domain. From this point of view, it consists in applying a multigrid method to the full optimization problem. A variant or extension of this approach is the MGOPT algorithm presented in [16, 17] which potentially allows for the treatment of non convex problems and inequality constraints in the optimization problem. The primary goal of these methods is however to solve the optimization problem on

the high resolution grid and the coarse grids are used only to accelerate the process. Thus the notion of local refinement is not present.

In this paper, we adapt the usual so-called 4D-Var data assimilation method and the use of the adjoint model to the case where the domain is locally refined. In section 2, we briefly remind the reader of the local mesh refinement method and introduce the data assimilation problem. In section 3, we derive the adjoint of the nested model. This adjoint system is derived both in the case of one-way and two-way interactions. Both methods are then evaluated in section 4 in the simple idealized testcase of a 1D nonlinear shallow water model.

2 LOCAL MESH REFINEMENT AND DATA ASSIMILATION

We limit our analysis to the simple generic case where there is only one high resolution grid covering a local domain ω embedded in a larger domain Ω at a coarser resolution as shown on figure 1.

[Figure 1 about here.]

The coarse model provides the boundary conditions to the high resolution domain on the common interface Γ. If this is the only data exchange between the two grids, the system is said to be in "one-way" (or passive) interaction. If, additionally, there is a feedback from the high resolution solution to the coarse resolution solution, the model is in "two-way" (or active) interaction. These interactions can be summarized in the following system which is written in the general two-way case:

$$\text{Coarse grid domain } \Omega_H \qquad \begin{cases} \dfrac{\partial \mathbf{x}_H}{\partial t} = F(\mathbf{x}_H, \mathbf{x}_\omega) \\ \mathbf{x}_H(t=0) = \mathbf{x}_H^0 \\ \mathbf{x}_\omega = G_h^H(\mathbf{x}_h) \end{cases} \tag{1}$$

$$\text{Fine grid domain } \omega_h \qquad \begin{cases} \dfrac{\partial \mathbf{x}_h}{\partial t} = F(\mathbf{x}_h, \mathbf{x}_{\partial\omega}) \\ \mathbf{x}_h(t=0) = \mathbf{x}_h^0 \\ \mathbf{x}_{\partial\omega} = I_H^h(\mathbf{x}_H) \end{cases} \tag{2}$$

where $\mathbf{x}_H^0$ and $\mathbf{x}_h^0$ are the initial conditions on both grids, $\mathbf{x}_{\partial\omega}$ stands for the boundary conditions on ω_h obtained by an interpolation of the coarse solution, I_H^h is an interpolation operator from Ω_H to $\partial\omega$. $\mathbf{x}_\omega$ is obtained by a restriction of the fine grid solution, G_h^H being the restriction operator from ω_h to Ω_H (it represents the feedback from the high to the coarse resolution grid in the case of two-way interaction). Note that, for sake of simplicity, we use the same operator F to represent the right hand side of the equations on both the coarse and fine grids. In practice, it can of course be different, at least at the discrete level.

After discretization, the problems have to be integrated in time in a specific order. The model is first integrated on the coarse grid Ω_H and then on the high resolution ω_h grid with boundary conditions given by a spatial and temporal interpolation of the coarse values. Finally a feedback can be applied. An example of this integration order with a time refinement factor of 2 is shown on figure (2).

[Figure 2 about here.]

The data assimilation problem

Starting from now, we assume that some observations $\mathbf{y}_H^o$ and $\mathbf{y}_h^o$ are available on both grids, and that we want to assimilate them into the nested system using a variational data assimilation technique. We have to define an *observation cost function* J^{obs} as the sum of the misfit between observations and corresponding model quantities over the coarse and fine domains:

$$\begin{aligned} J^{obs}(\mathbf{x}_H^0, \mathbf{x}_h^0) &= J_H^{obs}(\mathbf{x}_H^0, \mathbf{x}_h^0) + J_h^{obs}(\mathbf{x}_H^0, \mathbf{x}_h^0) \\ &= \frac{1}{2}\int_0^T \left\langle H_H(\mathbf{x}_H) - \mathbf{y}_H^{obs}, \mathbf{R}_H^{-1}\left(H_H(\mathbf{x}_H) - \mathbf{y}_H^{obs}\right)\right\rangle_{\Omega_H} \\ &\quad + \frac{1}{2}\int_0^T \left\langle H_h(\mathbf{x}_h) - \mathbf{y}_h^{obs}, \mathbf{R}_h^{-1}\left(H_h(\mathbf{x}_h) - \mathbf{y}_h^{obs}\right)\right\rangle_{\omega_h} \end{aligned} \tag{3}$$

where H_H (resp. H_h) is the observation operator on the coarse (resp. fine) resolution domain, linking the observations and the corresponding model quantities, $< .,. >_D$ is the usual Euclidian scalar product on a domain D, and $\mathbf{R}_H$ (resp. $\mathbf{R}_h$) is the covariance matrix associated with the observation error on $\mathbf{y}_H^{obs}$ (resp. $\mathbf{y}_h^{obs}$).

The goal is now to find the initial conditions on both grids $\mathbf{x}_H^0$ and $\mathbf{x}_h^0$ that minimize this cost function. This minimization will make use of the gradient of J^{obs}, which will be computed with the help of the adjoint model described in next section.

Observations errors and representativeness errors

The cost function given by (3) is the sum of the misfits between model solution and observations on both coarse and fine grids.
In two-way interaction, the coarse grid solution is updated in the area of the fine grid domain. So that in principle it should not be necessary to penalize the coarse grid solution to the observations in this area. However, removing this contribution corresponds to look at the model as a truly multiresolution model (sometimes called composite grids) and this implies developing the corresponding observations and background error covariance matrices. This is not performed in this paper where the numerical experiments will be done with observations and background covariance matrices defined independently on each grid. Development of truly multigrid background error covariance matrix is the main subject of the companion paper [14].
In one-way interaction, this can be fully justified to have, inside the fine grid domain, both the misfit to the coarse and fine grid solutions appearing in the cost function. However, for a given observation, the value of the error variance, that includes representativeness error, may differ on coarse and fine grids. In particular we can presume that the representativeness errors are larger on the coarse grid. However (as in every data assimilation experiment) the question of how to quantify these representativeness errors is difficult and will not be addressed here.

Background term

In practice, the cost function generally involves additional terms representing a penalization (relaxation of the optimal controls towards some background

values) or a regularization of the optimal controls : $J = J^{obs} + J^b$ where

$$J^b = \frac{1}{2} < \mathbf{x}_H^0 - x_H^b, B_H^{-1}\left(\mathbf{x}_H^0 - x_H^b\right) >_{\Omega_H} + \frac{1}{2} < \mathbf{x}_h^0 - x_h^b, B_h^{-1}\left(\mathbf{x}_h^0 - x_h^b\right) >_{\omega_h}$$

where B_H and B_h are the error covariance matrix of the background estimates. These terms can easily be incorporated to the previous formulation just by adding their contributions to the corresponding gradients.
One important question relies in a definition of error covariance matrices B_H and B_h that takes into account the multigrid aspect of the simulation. As already said, in this paper we will assume independent error covariance matrices.

3 THE ADJOINT OF THE NESTED MODEL

In this section, we derive the adjoint model corresponding to the nested system (1)-(2) introduced in the previous section. This derivation is performed in the general case of two-way interaction.

3.1 Derivation of the adjoint model

In the following, the usual way of deriving the adjoint model (e.g. [18]) is applied to the nested model. Let us introduce a couple of perturbations $(\delta\mathbf{x}_H^0, \delta\mathbf{x}_h^0)$ of the initial conditions on Ω_H and ω_h. The tangent linear models, involving the Gâteaux derivatives $\widehat{\mathbf{x}}_H$ and $\widehat{\mathbf{x}}_h$ of $\mathbf{x}_H$ and $\mathbf{x}_h$ are given by:

$$\text{Domain } \Omega_H \qquad \left\{ \begin{array}{l} \dfrac{\partial \widehat{\mathbf{x}}_H}{\partial t} = \dfrac{\partial F}{\partial \mathbf{x}_H}.\widehat{\mathbf{x}}_H + \dfrac{\partial F}{\partial \mathbf{x}_\omega}.\widehat{\mathbf{x}_\omega} = \dfrac{\partial F}{\partial \mathbf{x}_H}.\widehat{\mathbf{x}}_H + \dfrac{\partial F}{\partial \mathbf{x}_\omega}.\mathbf{G}_h^H\widehat{\mathbf{x}}_h \\ \widehat{\mathbf{x}}_H(0) = \delta\mathbf{x}_H^0 \end{array} \right. \tag{4}$$

$$\text{Domain } \omega_h \qquad \left\{ \begin{array}{l} \dfrac{\partial \widehat{\mathbf{x}}_h}{\partial t} = \dfrac{\partial F}{\partial \mathbf{x}_h}.\widehat{\mathbf{x}}_h + \dfrac{\partial F}{\partial \mathbf{x}_{\partial\omega}}.\widehat{\mathbf{x}}_{\partial\omega} = \dfrac{\partial F}{\partial \mathbf{x}_h}.\widehat{\mathbf{x}}_h + \dfrac{\partial F}{\partial \mathbf{x}_{\partial\omega}}.\mathbf{I}_H^h\widehat{\mathbf{x}}_H \\ \widehat{\mathbf{x}}_h(0) = \delta\mathbf{x}_h^0 \end{array} \right. \tag{5}$$

where we introduced the tangent linear operators $\mathbf{G}_h^H = \dfrac{\partial G_h^H}{\partial \mathbf{x}_h}$ and $\mathbf{I}_H^h = \dfrac{\partial I_H^h}{\partial \mathbf{x}_H}$.

Taking the scalar product of (4) by an adjoint variable $\mathbf{P}$ defined on Ω_H and integrating from time 0 to time T leads to:

$$\begin{aligned} \int_0^T < \frac{\partial \widehat{\mathbf{x}}_H}{\partial t}, \mathbf{P} >_{\Omega_H} &= \int_0^T < \frac{\partial F}{\partial \mathbf{x}_H}.\widehat{\mathbf{x}}_H + \frac{\partial F}{\partial \mathbf{x}_\omega}.\mathbf{G}_h^H\widehat{\mathbf{x}}_h, \mathbf{P} >_{\Omega_H} \\ &= \int_0^T < \widehat{\mathbf{x}}_H, \left[\frac{\partial F}{\partial \mathbf{x}_H}\right]^*.\mathbf{P} >_{\Omega_H} + \int_0^T < \widehat{\mathbf{x}}_h, \mathbf{G}_H^h.\left[\frac{\partial F}{\partial \mathbf{x}_\omega}\right]^*.\mathbf{P} >_{\omega_h} \end{aligned}$$

where $\mathbf{P}$ has been chosen equal to 0 on the boundary of Ω_H and where $\mathbf{G}_H^h$ is defined as the adjoint operator of $\mathbf{G}_h^H$.

Using the integration by parts in time:

$$\int_0^T < \frac{\partial \widehat{\mathbf{x}}_H}{\partial t}, \mathbf{P} >_{\Omega_H} = < \widehat{\mathbf{x}}_H(T), \mathbf{P}(T) >_{\Omega_H} - < \widehat{\mathbf{x}}_H(0), \mathbf{P}(0) >_{\Omega_H} - \int_0^T < \widehat{\mathbf{x}}_H, \frac{\partial \mathbf{P}}{\partial t} >_{\Omega_H}$$

one obtains

$$\int_0^T < \widehat{\mathbf{x}}_H, \frac{\partial \mathbf{P}}{\partial t} + \left[\frac{\partial F}{\partial \mathbf{x}_H}\right]^* . \mathbf{P} >_{\Omega_H} + \int_0^T < \widehat{\mathbf{x}}_h, \mathbf{G}_H^h . \left[\frac{\partial F}{\partial \mathbf{x}_\omega}\right]^* . \mathbf{P} >_{\omega_h} = \\ < \widehat{\mathbf{x}_H}(T), \mathbf{P}(T) >_{\Omega_H} - < \delta \mathbf{x}_H^0, \mathbf{P}(0) >_{\Omega_H} \tag{6}$$

Proceeding similarly on ω_h with an adjoint variable $\mathbf{Q}$, the following relation holds:

$$\int_0^T < \widehat{\mathbf{x}}_h, \frac{\partial \mathbf{Q}}{\partial t} + \left[\frac{\partial F}{\partial \mathbf{x}_h}\right]^* . \mathbf{Q} >_{\omega_h} + \int_0^T < \widehat{\mathbf{x}}_H, \mathbf{I}_h^H \left[\frac{\partial F}{\partial \mathbf{x}_{\partial\omega}}\right]^* . \mathbf{Q} >_{\Omega_H} = \\ < \widehat{\mathbf{x}}_h(T), \mathbf{Q}(T) >_{\omega_h} - < \delta \mathbf{x}_h^0, \mathbf{Q}(0) >_{\omega_h} \tag{7}$$

where $\mathbf{I}_h^H$ is the adjoint operator of $\mathbf{I}_H^h$.

The Gâteaux derivative of the objective function J^{obs} defined by (3) is given by

$$\begin{aligned} \hat{J}^{obs}(\mathbf{x}_H^0, \mathbf{x}_h^0, \delta\mathbf{x}_H^0, \delta\mathbf{x}_h^0) &= \int_0^T < \mathbf{H}_H \widehat{\mathbf{x}}_H, \mathbf{R}_H^{-1} \left(H_H(\mathbf{x}) - \mathbf{y}_H^{obs}\right) >_{\Omega_H} \\ &\quad + \int_0^T < \mathbf{H}_h \widehat{\mathbf{x}}_h, \mathbf{R}_h^{-1} \left(H_h(\mathbf{x}) - \mathbf{y}_h^{obs}\right) >_{\omega_h} \\ &= < \nabla_{\mathbf{x}_H^0} J^{obs}, \delta\mathbf{x}_H^0 > + < \nabla_{\mathbf{x}_h^0} J^{obs}, \delta\mathbf{x}_h^0 > \end{aligned}$$

where $\mathbf{H}_H = \dfrac{\partial H_H}{\partial \mathbf{x}_H}$ and $\mathbf{H}_h = \dfrac{\partial H_h}{\partial \mathbf{x}_h}$.

Choosing $\mathbf{P}(T) = \mathbf{Q}(T) = 0$ and summing (6) and (7) leads to :

$$\int_0^T < \widehat{\mathbf{x}}_H, \frac{\partial \mathbf{P}}{\partial t} + \left[\frac{\partial F}{\partial \mathbf{x}_H}\right]^* . \mathbf{P} + \mathbf{I}_h^H \left[\frac{\partial F}{\partial \mathbf{x}_{\partial\omega}}\right]^* . \mathbf{Q} >_{\Omega_H} \\ + \int_0^T < \widehat{\mathbf{x}}_h, \frac{\partial \mathbf{Q}}{\partial t} + \left[\frac{\partial F}{\partial \mathbf{x}_h}\right]^* . \mathbf{Q} + \mathbf{G}_H^h . \left[\frac{\partial F}{\partial \mathbf{x}_\omega}\right]^* . \mathbf{P} >_{\omega_h} \\ = - < \delta \mathbf{x}_H^0, \mathbf{P}(0) >_{\Omega_H} - < \delta \mathbf{x}_h^0, \mathbf{Q}(0) >_{\omega_h}$$

Therefore the choice of $\mathbf{P}$ and $\mathbf{Q}$ as solutions of the following systems:

Domain Ω_H

$$\begin{cases} \dfrac{\partial \mathbf{P}}{\partial t} + \left[\dfrac{\partial F}{\partial \mathbf{x}_H}\right]^* . \mathbf{P} + \mathbf{I}_h^H \left[\dfrac{\partial F}{\partial \mathbf{x}_{\partial\omega}}\right]^* . \mathbf{Q} = \mathbf{H}_H^* \mathbf{R}_H^{-1} \left(H_H(\mathbf{x}) - \mathbf{y}_H^{obs}\right) \\ \mathbf{P}(T) = 0 \\ \mathbf{P}_{|\partial\Omega_H} = 0 \end{cases} \tag{8}$$

Domain ω_h

$$\begin{cases} \dfrac{\partial \mathbf{Q}}{\partial t} + \left[\dfrac{\partial F}{\partial \mathbf{x}_h}\right]^* . \mathbf{Q} + \mathbf{G}_H^h . \left[\dfrac{\partial F}{\partial \mathbf{x}_\omega}\right]^* . \mathbf{P} = \mathbf{H}_h^* \mathbf{R}_h^{-1} \left(H_h(\mathbf{x}) - \mathbf{y}_h^{obs}\right) \\ \mathbf{Q}(T) = 0 \\ \mathbf{Q}_{|\partial\omega_h} = 0 \end{cases} \tag{9}$$

leads to the gradients of the cost function J^{obs}:

$$\begin{cases} \nabla_{\mathbf{x}_H^0} J^{obs} = -\mathbf{P}(0) \\ \nabla_{\mathbf{x}_h^0} J^{obs} = -\mathbf{Q}(0) \end{cases}$$

This system (8)-(9) is the adjoint version of the two-way direct model. There is also a two-way interaction in this system and the two grids must be integrated simultaneously. The discrete version of this algorithm is detailed in appendix.

3.2 Simplifications for the one-way case and off-line coupling

In the special case of one-way interaction, the preceding system is simplified as follows :

$$\text{Domain } \Omega_H \qquad \left\{ \begin{array}{l} \dfrac{\partial \mathbf{P}}{\partial t} + \left[\dfrac{\partial F}{\partial \mathbf{x}_H}\right]^* .\mathbf{P} + \mathbf{I}_h^H \left[\dfrac{\partial F}{\partial \mathbf{x}_{\partial\omega}}\right]^* .\mathbf{Q} = \mathbf{H}_H^* \mathbf{R}_H^{-1} \left(H_H(\mathbf{x}) - \mathbf{y}_H^{obs}\right) \\ \mathbf{P}(T) = 0 \\ \mathbf{P}_{|\partial\Omega_H} = 0 \end{array} \right. \tag{10}$$

$$\text{Domain } \omega_h \qquad \left\{ \begin{array}{l} \dfrac{\partial \mathbf{Q}}{\partial t} + \left[\dfrac{\partial F}{\partial \mathbf{x}_h}\right]^* .\mathbf{Q} = \mathbf{H}_h^* \mathbf{R}_h^{-1} \left(H_h(\mathbf{x}) - \mathbf{y}_h^{obs}\right) \\ \mathbf{Q}(T) = 0 \\ \mathbf{Q}_{|\partial\omega_h} = 0 \end{array} \right. \tag{11}$$

We can observe a feedback term from the high resolution adjoint solution onto the coarse resolution adjoint solution, in an opposite way in comparison with the direct one-way model. Due to this feedback, the adjoint model should here be first integrated on the high resolution grid. Under the assumption that this order is satisfied, the coarse and high resolution adjoint models can be integrated independently. So that the preceding system of adjoint equations, along with eqns (1)-(2) corresponding to the forward models, provides a consistent way of running a coarse resolution model and an embedded high resolution model, both of them assimilating data. From a practical point of view, the coupling between the high and low resolution adjoint and direct models can be made "off-line".

4 APPLICATION TO A 1-D SHALLOW WATER SYSTEM

We present here the application of the preceding methods to the idealized context of twin experiments within a 1-D shallow water model. This system is representative of gravity waves propagation in a thin layer of homogeneous water. Besides its physical relevance, it also presents the interest, when discretized on a staggered grid, to require interpolation steps despite the fact that the problem is only 1-D. The data assimilation methods described in the previous section are applied.

4.1 The shallow water equations and their discretization

In the following, ϕ denotes the water height, u the velocity, ν the viscosity coefficient, C the bottom friction coefficient and z_b the height of the bottom profile. The shallow water equations are written under the following form:

$$\left\{ \begin{array}{l} \dfrac{\partial \phi}{\partial t} + \dfrac{\partial (\phi u)}{\partial x} = 0 \\ \dfrac{\partial u}{\partial t} + \dfrac{\partial}{\partial x}\left(\dfrac{1}{2}u^2 + g(\phi + z_b)\right) = \nu \dfrac{\partial^2 u}{\partial x^2} - Cu \end{array} \right. \tag{12}$$

along with associated initial and boundary conditions.

Discretization

This model is discretized on a staggered grid with water height ϕ located at the center of the cells and velocity u at the nodes (figure 3). Spatial derivatives are approximated by standard second order centered methods. Numerical stability is achieved by using a forward-backward temporal scheme.

In this experiment, boundary conditions are implemented by imposing the water height and the velocity at the boundaries as shown in bold on figure 3.

[Figure 3 about here.]

4.2 Configuration of the numerical model

One justification for using grid refinement could come from the need for a better representation of the domain. For example, in ocean or atmosphere modelling, the topography will be better represented at higher resolution. The following experiments are driven by this case where a strong topographic feature is hardly represented on the coarse grid.

Grid parameters

The extent of the global (coarse resolution) domain is $L = 1000$m, with a spatial resolution of 10m, so that 100 cells are needed to discretize the coarse grid domain. This coarse domain is closed at its boundaries by setting velocities to zero.

The numerical experiments are performed with one fixed refined grid, located at the center of the global domain and which size is $L/4 = 250$m (figure 4). The mesh refinement factor is equal to 5, leading to a resolution of 2m and a high resolution grid composed of 125 cells. The time step is $\Delta t = 0.01$s and is the same for both grids (there is no time refinement).

[Figure 4 about here.]

Physical parameters

The values of the viscosity and friction coefficients are set to 0.1 $\mathrm{m}^2.\mathrm{s}^{-1}$ and $10^{-4}\mathrm{s}^{-1}$. The bottom topography has a Gaussian shape: $z_b(x) = z_0 \exp\left[-(x - L/2)^2/50\right]$ with $z_0 = 5$ m. The discrete topography is then smoothed according to the grid resolution following the criterion (usual in ocean and atmosphere applications):

$$\max_i \frac{|z_b(i) - z_b(i-1)|}{|z_b(i) + z_b(i-1)|} \leq r_{\max} = 0.05$$

In realistic experiments, this smoothing criterion is applied with the objective to lower the so-called gradient pressure error arising in terrain following vertical coordinate models. The discrete topography obtained on fine and coarse grids after smoothing is plotted on figure 5.

[Figure 5 about here.]

Nesting parameters

The nesting schemes are the most simple ones: we use clamped boundary conditions on the high resolution grid (copy of the coarse grid value for velocity and linear interpolation for water elevation), and the restriction operator is an injection (copy at corresponding grid points). Better grid interactions based on characteristic variables (e.g. [19]) could also have been chosen.

4.3 Configuration of the assimilation experiments

Reference experiment

A reference experiment was run using a single grid covering the whole domain $[0, L]$ with a uniformly high resolution of 2m. The model was integrated over a time period of 5 minutes, with the initial conditions: $u(x, t = 0) = \sin(\pi x/L)$ and $\phi(x, t = 0) + z_b(x) = H_0$ with $H_0 = 10$m. The solution of this reference experiment will be considered as the "truth" in the following, and will be used to generate pseudo observations for the assimilation experiments, and also to compute the errors of the solutions of the one- and two-way cases obtained after assimilation.

Observations

We suppose in our numerical experiments that observations of the water height ϕ only are available and that we do not have access to observations of the velocity. These observations are coming from the reference solution, sampled every 40m in space and every 60 time steps. Thus we have one observation every 20 grid points on the high resolution grid and every 4 grids points on the coarse resolution grid. Note that experiments conducted with other densities of observations lead to the same conclusions (not shown). A uniform white noise is then added to water height observations with a standard deviation of 20cm which corresponds to a perturbation amplitude of approximatively 10%.

Moreover we assume that the observation errors are independent (R_H and R_h are diagonal matrices) and their constant coefficient is equal to the variance of 0.04. Note that by choosing the same variance for both coarse and fine, we assume the same representativeness errors on both grids (actually 0 in our case).

First guess for the initial conditions

A simulation was conducted on a single grid version of the model covering the whole domain $[0, L]$ with a very coarse resolution of 50m (five times larger than the resolution of the coarse grid in the nested experiments). This simulation used the same analytical initial condition than indicated previously. Then the solution at $t = 5$ minutes was interpolated both on Ω_H and ω_h and taken as the first guess for the initial conditions in the assimilation experiments. This first guess is plotted on figure 6, along with the corresponding reference solution.

[Figure 6 about here.]

Background term and cost function

In order to regularize the problem, a background term J^b is added to the cost function. J^b has the form of a smoothing operator written as :

$$J^b = G(u_{0,H}, u_{b,H}, \sigma^u_{b,H}, l^u_{b,H}) + G(\phi_{0,H}, \phi_{b,H}, \sigma^\phi_{b,H}, l^\phi_{b,H}) + G(u_{0,h}, u_{b,h}, \sigma^u_{b,h}, l^u_{b,h}) + G(\phi_{0,h}, \phi_{b,h}, \sigma^\phi_{b,h}, l^\phi_{b,h})$$

with

$$G(X_0, X_b, \sigma_b, l) = \frac{1}{2\sqrt{2}{\sigma_b}^2 l} \left[\|X_0 - X_b\|^2 + \left\| l^2 \frac{\mathrm{d}^2}{\mathrm{d}x^2}(X_0 - X_b) \right\|^2 \right]$$

It can be shown (see [20]) that, in term of background error covariance matrix B, this approximates a Gaussian error covariance matrix with a variance of ${\sigma_b}^2$ and a correlation length of l.
In the numerical experiments, the following values of the different parameters will be used :

$$\sigma^u_{b,H} = \sigma^u_{b,h} = 0.1\mathrm{m.s}^{-1}, \qquad \sigma^\phi_{b,H} = \sigma^\phi_{b,h} = 0.15\mathrm{m}, \qquad l^u_{b,H} = l^u_{b,h} = l^\phi_{b,H} = l^\phi_{b,h} = 50\mathrm{m}$$

Optimization algorithm

The optimization is done with a truncated quasi Newton algorithm based on the m1qn3 routine [21]. The stopping criterion is given by $\|\nabla J\|/\|\nabla J_0\| \leq \epsilon$ where $\epsilon = 10^{-3}$ and where ∇J_0 is the initial value of the gradient of the cost function.

5 NUMERICAL RESULTS

5.1 Reference solution

The time evolution of the reference solution is plotted on figures 8, 7. At a given point, the water height level oscillates between large and small values around the central point of the domain which corresponds to the location of the top of the seamount. At the top of the seamount, small scales perturbations are observed.

[Figure 7 about here.]

[Figure 8 about here.]

5.2 Quality of the identified solution

Cost function

The evolution of the cost functions during the minimization is indicated on figure 9. As expected, the final value is much smaller for the two-way case.

[Figure 9 about here.]

Results on the fine grid ω_h

The root mean square (RMS) error on the high resolution grid is computed by comparing the solutions provided by the assimilation procedures and the reference solution at each grid point in time and space

$$RMS(z) = \sqrt{\frac{1}{T|\omega_h|} \int_0^T \|z - z^{ref}\|^2_{\omega_h}}$$

where z is either u or ϕ. The RMS errors given by the different methods are displayed in figure 10. The value at the first iteration gives the error produced by one-way and two-way nesting without assimilation. Even if the grid interactions are very crude (clamped boundary conditions), the two-way nesting algorithm performs (slightly) better.

After assimilation, the two-way simulation attains a much lower level of error than the one-way simulation, especially for the non observed variable (the velocity). This is due in particular to the fact that, in the one-way experiment, the coarse grid is not able to represent correctly the bottom profile due to its lower resolution. Therefore the assimilation process decreases the error in the boundary conditions provided by the coarse grid but not enough to get a solution as accurate as with the two-way algorithm.

[Figure 10 about here.]

Results on the coarse grid Ω_H

The ability to improve the coarse grid solution is an important aspect in such nested systems. Figure 11 represents the RMS error computed on $\Omega_H \setminus \omega_H$, i.e. the part of the coarse grid domain not covered by the fine grid domain. It appears that during the experiment, RMS errors either on velocity or on water height have been divided by a factor of roughly 10 in the one-way case. If we remember that there is no feedback from the fine grid onto the coarse grid in the direct model in this case, this result illustrates the importance of the feedback term which appears is the adjoint formulation (10). In the two-way case, the accuracy of the identified solution on the coarse grid is even better, which is due to the strong coupling between both grids, either in the direct and in the adjoint models.

[Figure 11 about here.]

Impact of the location of observations

In this last series of experiments, we compare solutions obtained with observations located only on the fine grid domain and observations located on both coarse and fine grids domains. Figures 12 and 13 compare the spatial RMS errors obtained, after convergence of the minimization, for water height and velocity for these two different cases. The plotted RMS error are averages over the whole time period :

$$RMS(z)(x) = \sqrt{\frac{1}{T} \int_0^T \left(z(x,t) - z^{ref}(x,t)\right)^2 \mathrm{d}t}$$

where z is either u or ϕ.
For the one-way experiment, there are two curves since, to the contrary of the two-way case, the coarse and fine grid solutions in the fine grid domain differ. Best performance is of course obtained in the two-way case with observations on the whole domain. When observations are located only on the fine grid domain, the behavior of two-way simulations is similar with a higher level of error.
The one-way experiments deserve more discussion. First, in one-way, nothing ensures in the numerical algorithm a solution with continuous derivatives at the coarse/fine grid interfaces. Jumps in the RMS water height fields, which corresponds to jumps in the solutions, are indeed clearly visible, in particular when observations are located everywhere (continuous lines). Second, since there is no feedback from the fine to the coarse grid solution, the improvement of the coarse and fine grid solutions compete to the minimization of the global cost function which is the sum of the misfit on coarse and fine grids. In this experiment, in some part of the fine grid domain, it's even lead to a RMS error smaller on the coarse grid solution than on the fine grid solution . The question of how to weight the observations, by specifying judicious observations error covariance matrices, in order to get the best solution on the fine grid is difficult to answer. The largest level of RMS errors are obtained when observations are located only on the fine grid domain. However in that case the one-way solution presents less discontinuities : even if at different resolutions, the initial controls on both coarse and fine grid are computed by minimizing a misfit with observations located in the same domain (the fine grid domain). These experiments tend to show the need for a better definition of multiresolution error covariance matrices, especially for one-way interaction. This is one of the subjects of [14].

[Figure 12 about here.]

[Figure 13 about here.]

6 SUMMARY AND FUTURE WORK

We addressed in this paper the problem of 4D variational data assimilation in the context of locally nested models. Such systems are more and more frequently used in ocean and atmosphere applications, either to improve locally the model solution in areas of particular interest or, in the case of two-way interaction, to improve the global coarse grid model solution . Since data assimilation is presently becoming a fundamental aspect of any forecasting system, it is therefore necessary to be able to consistently assimilate data in such nested models. Moreover another potential reason for increasing resolution is when very high resolution observations are locally available and coarse resolution models are not able to represent such high resolution features. In this case, the choice of the high resolution grid location would be dictated by the location of observations.

We have introduced an algorithm for 4D variational data assimilation in such a context of a local mesh refinement. This formulation is obtained, in both the one- and two-way cases, by a direct derivation of the adjoint of the two level algorithm. Numerical experiments in the very idealized test case of a 1D

shallow water model tend to show that this approach performs well and leads to a fast convergence rate.

The aim of this paper was only to introduce these methods. It is however clear that this approach can be improved and that important issues are still to be discussed. In particular, in one-way simulations, a consistent choice of observation operators and covariance matrices of the observations errors specified on the coarse and fine grids may be crucial in realistic applications. This question is also directly related to the choice of the appropriate density of observations as a function of the grid resolution. Finally, this general variational approach also gives the possibility to include, in the cost function, physical constraints at grid interfaces in order to improve the nesting method. Several of these aspects are addressed in a companion paper [14], as well as more demanding numerical experiments in a 2D case.

Derivation of the discrete adjoint models

Let Ω_H and ω_h be the discrete domains at coarse and high resolutions. $\overset{\circ}{\Omega}_H$ and $\overset{\circ}{\omega}_h$ denote the sets composed of strictly interior points only. Additionally $\overset{\circ}{\omega}_H$ denotes the coarse grid points interior to the high resolution domain ω. The time interval $[0:T]$ is divided into N_t time steps. We describe here the discrete version of the two-way adjoint models. The assumption is also made that the model is discretized with an explicit first order temporal scheme.

The discrete models are written under the following general form :

$$\left\{ \begin{array}{ll} Y_i^{n+1} = F_H(Y_i^n) & \forall i \in \overset{\circ}{\Omega}_H \\ Y_i^{n+1} = (DZ^{n+1})_i & \forall i \in \overset{\circ}{\omega}_H \quad \text{(update)} \end{array} \right.$$

$$\left\{ \begin{array}{ll} {Z_i}^{n+1} = F_h(Z_i^n) & \forall i \in \overset{\circ}{\omega}_h \\ {Z_i}^{n+1} = (CY^{n+1})_i & \forall i \in \partial\omega_h \text{ (interpolation)} \end{array} \right.$$

from which we derive the discrete tangent linear models :

$$\left\{ \begin{array}{ll} \hat{Y}_i^{n+1} = (A\hat{Y}^n)_i & \forall i \in \overset{\circ}{\Omega}_H \\ \hat{Y}_i^{n+1} = (D\hat{Z}^{n+1})_i & \forall i \in \overset{\circ}{\omega}_H \quad \text{(update)} \end{array} \right.$$

$$\left\{ \begin{array}{ll} \hat{Z}_i^{n+1} = (B\hat{Z}^n)_i & \forall i \in \omega_h \\ \hat{Z}_i^{n+1} = (C\hat{Y}^{n+1})_i & \forall i \in \partial\omega_h \text{ (interpolation)} \end{array} \right.$$

On Ω_H:

Let p be a discrete variable defined on the domain $\overset{\circ}{\Omega}_H$. Summing over time and space leads to:

$$\sum_{n=0}^{N_t-1} \sum_{i \in \overset{\circ}{\Omega}_H} p_i^{n+1} \hat{Y}_i^{n+1} = \sum_{n=0}^{N_t-1} \sum_{i \notin \overset{\circ}{\omega}_H} p_i^{n+1} (A\hat{Y}^n)_i + \sum_{n=0}^{N_t-1} \sum_{i \in \overset{\circ}{\omega}_H} p_i^{n+1} (D\hat{Z}^{n+1})_i$$

After discrete time integration by parts and setting $p_i^{N_t} = 0$, we get

$$\sum_{n=0}^{N_t-1} \sum_{i \in \overset{\circ}{\Omega}_H} p_i^n \hat{Y}_i^n - \sum_{i \in \overset{\circ}{\Omega}_H} p_i^0 \hat{Y}_i^0 = \sum_{n=0}^{N_t-1} \sum_{i \notin \overset{\circ}{\omega}_H} p_i^{n+1} (A\hat{Y}^n)_i + \sum_{n=0}^{N_t-1} \sum_{i \in \overset{\circ}{\omega}_H} p_i^{n+1} (D\hat{Z}^{n+1})_i$$

Then we introduce an auxiliary variable v defined on the coarse grid domain $\overset{\circ}{\Omega}_H$ by $v_i^{n+1} = p_i^{n+1}$, $\forall i \in \overset{\circ}{\Omega}_H \setminus \overset{\circ}{\omega}_H$ and $v_i^{n+1} = 0$, $\forall i \in \overset{\circ}{\omega}_H$. Then the following relation holds:

$$\sum_{n=0}^{N_t-1} \sum_{i \notin \overset{\circ}{\omega}_H} p_i^{n+1} (A\hat{Y}^n)_i = \sum_{n=0}^{N_t-1} \sum_{i \in \overset{\circ}{\Omega}_H} (A^T v^{n+1})_i \hat{Y}_i^n$$

so that

$$\begin{aligned}\sum_{n=0}^{N_t-1}\sum_{i\in\mathring{\Omega}_H} p_i^n\hat{Y}_i^n &= \sum_{n=0}^{N_t-1}\sum_{i\in\mathring{\Omega}_H}(A^T v^{n+1})_i\hat{Y}_i^n + \sum_{n=0}^{N_t-1}\sum_{i\in\mathring{\omega}_H} p_i^{n+1}(D\hat{Z}^{n+1})_i + \sum_{i\in\mathring{\Omega}_H} p_i^0\hat{Y}_i^0 \\ &= \sum_{n=0}^{N_t-1}\sum_{i\in\mathring{\Omega}_H}(A^T v^{n+1})_i\hat{Y}_i^n + \sum_{n=0}^{N_t-1}\sum_{i\in\mathring{\omega}_h}(D^T p^n)_i\hat{Z}_i{}^n \\ &\qquad + \sum_{i\in\mathring{\Omega}_H} p_i^0\hat{Y}_i^0 - \sum_{i\in\mathring{\omega}_h}(D^T p^0)_i\hat{Z}_i{}^0\end{aligned}$$

On ω_h:
Taking the scalar product by an adjoint variable q and using $q_i^{N_t}=0,\forall i$

$$\begin{aligned}\sum_{n=0}^{N_t-1}\sum_{i\in\mathring{\omega}_h} q_i^n\hat{Z}_i^n &= \sum_{n=0}^{N_t-1}\sum_{i\in\mathring{\omega}_h} q_i^{n+1}Z_i^{n+1} + \sum_{i\in\mathring{\omega}_h} q_i^0\hat{Z}_i^0 \\ &= \sum_{n=0}^{N_t-1}\sum_{i\in\mathring{\omega}_h} q_i^{n+1}(B\hat{Z}^n)_i + \sum_{i\in\mathring{\omega}_h} q_i^0\hat{Z}_i^0\end{aligned}$$

$$\begin{aligned}\sum_{n=0}^{N_t-1}\sum_{i\in\mathring{\omega}_h} q_i^{n+1}(B\hat{Z}^n)_i &= \sum_{n=0}^{N_t-1}\sum_{i\in\omega_h}(B^T q^{n+1})_i\hat{Z}_i^n \\ &= \sum_{n=0}^{N_t-1}\sum_{i\in\mathring{\omega}_h}(B^T q^{n+1})_i\hat{Z}_i^n + \sum_{n=0}^{N_t-1}\sum_{i\in\partial\omega_h}(B^T q^{n+1})_i(C\hat{Y}^n)_i \\ &= \sum_{n=0}^{N_t-1}\sum_{i\in\mathring{\omega}_h}(B^T q^{n+1})_i\hat{Z}_i^n + \sum_{n=0}^{N_t-1}\sum_{i\in\omega_H} C^T(B^T q^{n+1})_i\hat{Y}_i^n\end{aligned}$$

The discrete adjoint models are then given by:

$$\begin{cases} v_i^{n+1} = p_i^{n+1} \quad \forall i\in\mathring{\Omega}_H\setminus\mathring{\omega}_H, \quad v_i^{n+1}=0 \quad \forall i\in\mathring{\omega}_H \\ p_i^n = (A^T v^{n+1})_i + (C^T B^T q^{n+1})_i + (y-y_{obs}) \quad \forall i\in\mathring{\Omega}_H \\ q_i^n = (B^T q^{n+1})_i + (D^T p^n)_i + (z-z_{obs}) \quad \forall i\in\mathring{\omega}_h, \quad q_i^n=0 \quad \forall i\in\omega_h\setminus\mathring{\omega}_h \end{cases}$$

where y_{obs} and z_{obs} denote the observations on the coarse and fine grids respectively.
It can be implemented as follows:

1. Set v_i^{n+1}:

$$v_i^{n+1} = p_i^{n+1} \quad \forall i\in\mathring{\Omega}_H\setminus\mathring{\omega}_H, \quad v_i^{n+1}=0 \quad \forall i\in\mathring{\omega}_H$$

2. Compute p_i^n, q_i^n using the usual (monogrid) adjoint models:

$$\begin{cases} p_i^{n,} = (A^T v^{n+1})_i \quad \forall i\in\mathring{\Omega}_H \\ q_i^n = (B^T q^{n+1})_i \quad \forall i\in\mathring{\omega}_h, \quad q_i^n=0 \quad \forall i\in\omega_h\setminus\mathring{\omega}_h \end{cases}$$

3. Add the contributions of intergrid transfer operators and of observations:

$$\begin{cases} p_i^n = p_i^n + (C^T q^n)_i + (y - y_{obs}) & \forall i \in \mathring{\Omega}_H \\ q_i^n = q_i^n + (D^T p^n)_i + (z - z_{obs}) & \forall i \in \mathring{\omega}_h, \quad q_i^n = 0 \quad \forall i \in \omega_h \backslash \mathring{\omega}_h \end{cases}$$

It is important to note that the observations y_{obs} are actually not used inside the domain ω. This is natural since the coarse grid solution is updated in this area. The gradient of the cost function with regard to Y^0 will actually be zero everywhere in the high resolution domain, except for a few points. The number of points inside ω where the gradient is non zero depends on the size of the stencil of the matrix A.

Note that in the particular case of one-way interaction, the auxiliary variable v is not used and the discrete adjoint models are given by

$$\begin{cases} p_i^n = (A^T p^{n+1})_i + (C^T B^T q^{n+1})_i + (y - y_{obs}) \\ q_i^n = (B^T q^{n+1})_i + (z - z_{obs}) \end{cases}$$

References

[1] Levin JC, Iskandarani M, Haidgovel DB. To continue or discontinue: Comparisons of continuous and discontinuous Galerkin formulations in a spectral element ocean model. *Ocean Modelling* 2006; **15(1-2)**: 56-70.

[2] Fang F, Pain CC, Piggott MD , Gorman GJ, Goddard AJH. An adaptive mesh adjoint data assimilation method applied to free surface flows. *International Journal for Numerical Methods in Fluids* 2005; **47(8-9)**: 995-1001.

[3] Debreu L, Blayo E. Two-way embedding algorithms: a review. *Ocean Dynamics* 2008; **58**: 415:418

[4] Fox AD, Maskell SJ. Two-way interactive nesting of primitive equation ocean models with topography. *Journal of Physical Oceanography* 1995; **25**: 2977-2996.

[5] Kurihara YG, Tripoli GJ, Bender MA. Design of a movable nested-mesh primitive equation model. *Monthly Weather Review* 1979; **107** : 239-249.

[6] Oey LY, Chen P. A nested-grid ocean model with application to the simulation of meanders and eddies in the Norwegian coastal current. *Journal of Geophyical Research* 1992; **97**: 20063-20086.

[7] Spall MA, Holland WR. A nested primitive equation model for ocean applications. *Journal of Physical Oceanography* 1991; **21**: 205-220.

[8] Zhang DL, Chang HR, Seaman NL, Warner TT, Fritsch JM. A two way interactive nesting procedure with variable terrain resolution. *Monthly Weather Review* 1986; **114**: 1330-1339.

[9] Berger M, Oliger J. Adaptive mesh refinement for hyperbolic partial differential equations. *Journal of Computational Physics* 1984; **53**: 484-512.

[10] Skamarock WC, Klemp JB. Adaptive grid refinement for two-dimensional and three-dimensional nonhydrostatic atmospheric flows. *Monthly Weather Review* 1989; **121**: 788-804.

[11] Blayo E, Debreu L. Adaptive mesh refinement for finite difference ocean models: first experiments. *Journal of Physical Oceanography* 1999; **29**: 1239-1250.

[12] Rowley C, Ginis I. Implementation of a mesh movement scheme in a multiply nested ocean model and its application to air-sea interaction studies. *Monthly Weather Review* 1999; **127**: 1879-1896.

[13] Debreu L, Blayo E, Barnier B. A general adaptive multi-resolution approach to ocean modelling: experiments in a primitive equation of the north Atlantic. In Adaptive Mesh Refinement - Theory and Applications, Lecture Notes in Computer Science, Vol. 41, Plewa, Tomasz, Linde, Timur, Weirs, V. Gregory (Eds) 2005; 554 pp.

[14] Simon E, Debreu L, Blayo E. 4D variational data assimilation for locally nested models: complementary theoretical aspects and application to a 2D shallow water model. *International Journal for Numerical Methods in Fluids* 2009. submitted.

[15] Ta'asan S. One shot methods for optimal control of distributed parameters systems I:Finite dimensional control. *ICASE Report*, No. 91-2 (1991)

[16] Nash SG. A Multigrid Approach to Discretized Optimization Problems. *Journal of Optimization Methods and Software* 2000; **14**: 99-116.

[17] Lewis RM, Nash SG. Model Problems for the Multigrid Optimization of systems governed by differential equations. *SIAM Journal on Scientific Computing* 2005; **26-6**: 1811-1837.

[18] Le Dimet FX, Talagrand O. Variational algorithms for analysis and assimilation of meteorological observations: theoretical aspects. *Tellus* 1986; **38A**: 97-110.

[19] Blayo E, Debreu L. Revisiting open boundary conditions from the point of view of characteristic variables. *Ocean Modelling* 2005; **9**: 231-252.

[20] Bennett A. Inverse Modeling of the Ocean and Atmosphere, *Cambridge University Press* 2002; 225pp.

[21] Gilbert JC, Lemaréchal C. Some numerical experiments with variable storage quasi-Newton algorithms. *Mathematical Programming* 1989; **B25**: 407-435.

Centre de recherche INRIA Grenoble – Rhône-Alpes
655, avenue de l'Europe - 38334 Montbonnot Saint-Ismier (France)

Centre de recherche INRIA Bordeaux – Sud Ouest : Domaine Universitaire - 351, cours de la Libération - 33405 Talence Cedex
Centre de recherche INRIA Lille – Nord Europe : Parc Scientifique de la Haute Borne - 40, avenue Halley - 59650 Villeneuve d'Ascq
Centre de recherche INRIA Nancy – Grand Est : LORIA, Technopôle de Nancy-Brabois - Campus scientifique
615, rue du Jardin Botanique - BP 101 - 54602 Villers-lès-Nancy Cedex
Centre de recherche INRIA Paris – Rocquencourt : Domaine de Voluceau - Rocquencourt - BP 105 - 78153 Le Chesnay Cedex
Centre de recherche INRIA Rennes – Bretagne Atlantique : IRISA, Campus universitaire de Beaulieu - 35042 Rennes Cedex
Centre de recherche INRIA Saclay – Île-de-France : Parc Orsay Université - ZAC des Vignes : 4, rue Jacques Monod - 91893 Orsay Cedex
Centre de recherche INRIA Sophia Antipolis – Méditerranée : 2004, route des Lucioles - BP 93 - 06902 Sophia Antipolis Cedex

Éditeur
INRIA - Domaine de Voluceau - Rocquencourt, BP 105 - 78153 Le Chesnay Cedex (France)
http://www.inria.fr
ISSN 0249-6399

List of Figures

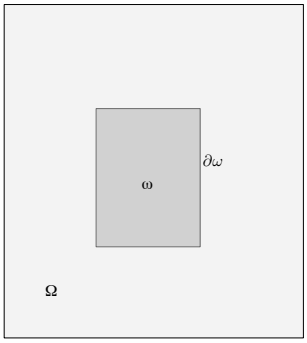

Figure 1: Domains covered by the coarse and high resolution grids

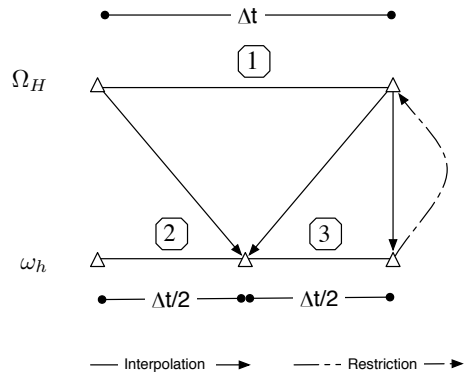

Figure 2: Integration of the two grids over one coarse grid time step Δt in the case of a time refinement ratio equal to 2. At time $t+\Delta t/2$, a linear interpolation in time occurs using values of the coarse grid at times t and $t + \Delta t$

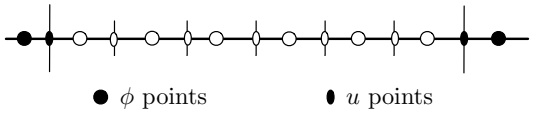

Figure 3: Staggered discretization grid. In black, points on which the boundary conditions are applied

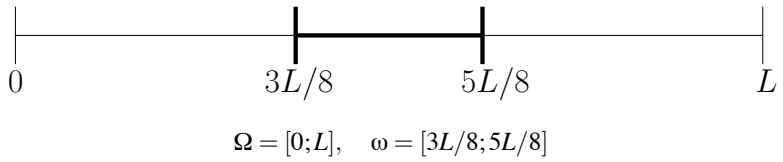

Figure 4: Location of the coarse and high resolution grids Ω_H and ω_h

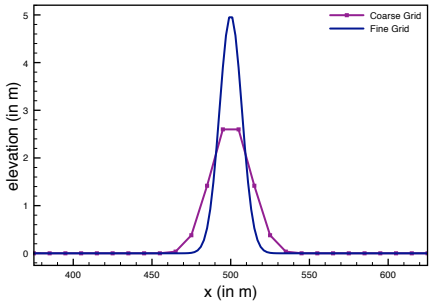

Figure 5: Discrete topography after smoothing (the nested domain only is shown)

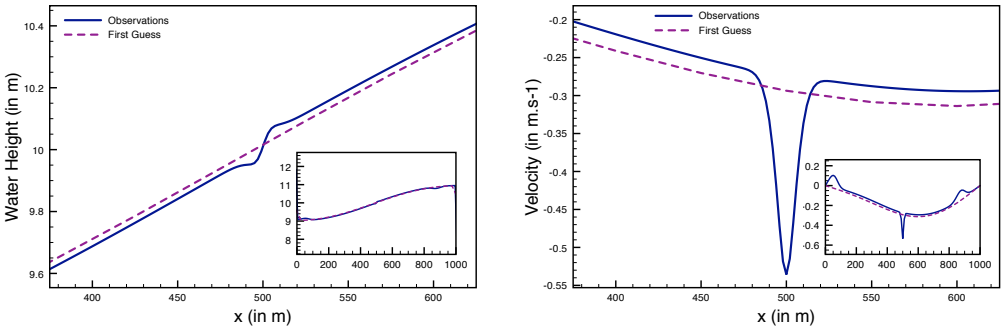

Figure 6: Initial conditions: first guess and reference solution(observations) on domain ω for the water height (left) and the velocity (right). Small frame: same on Ω.

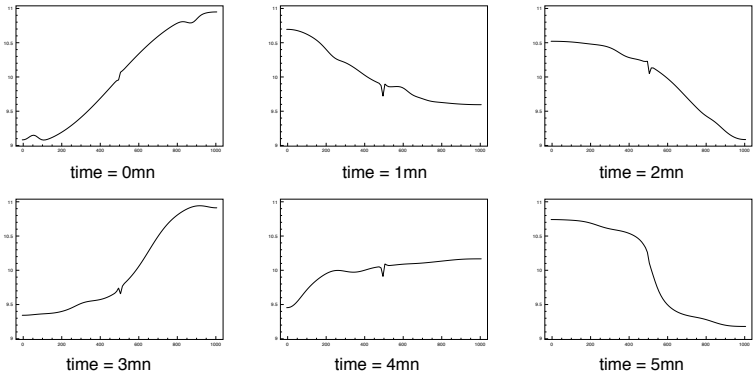

Figure 7: Time evolution of the water height (in m), snapshot every minute

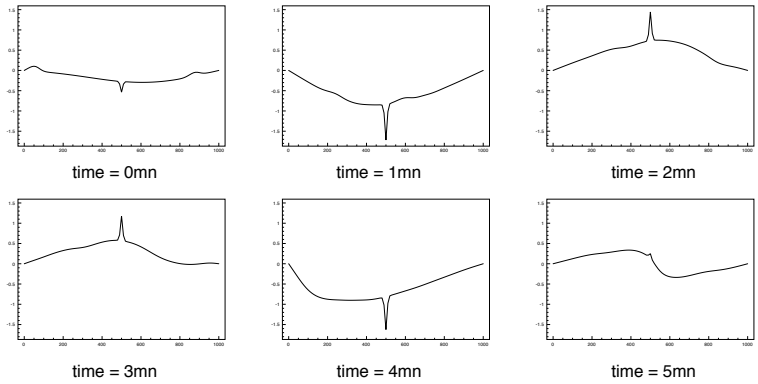

Figure 8: Time evolution of the velocity (in $\mathrm{m.s}^{-1}$), snapshot every minute

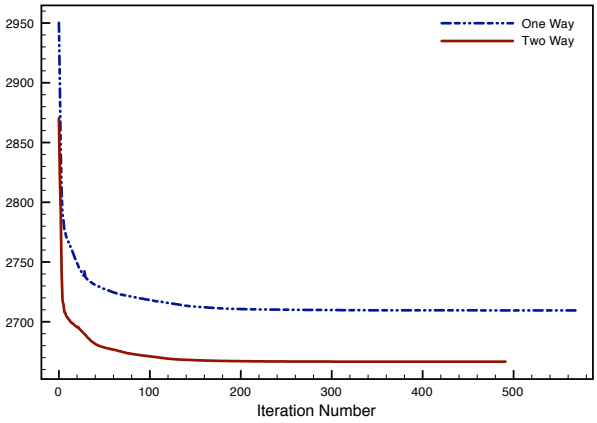

Figure 9: Evolution of the cost function as a function of the number of iterations

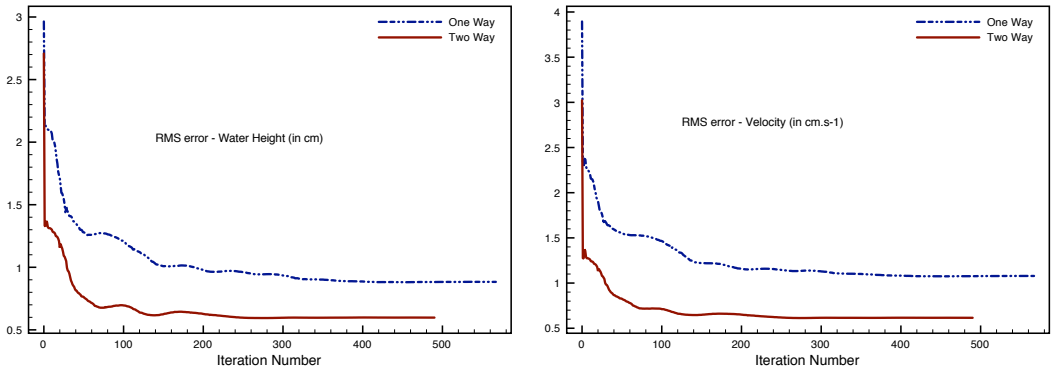

Figure 10: RMS error on the fine grid domain as a function of the iteration number: water height (left, in cm) and velocity (right, in $cm.s^{-1}$)

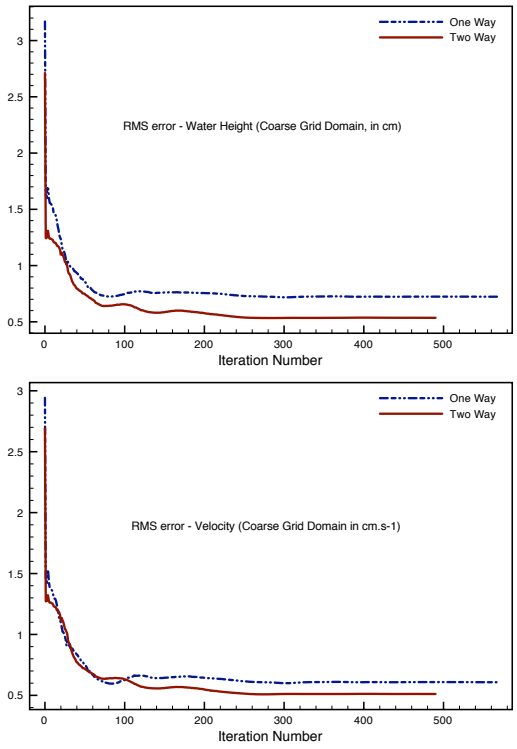

Figure 11: RMS error on the coarse grid $\Omega_H \setminus \omega_H$: water height (left, in cm) and velocity (right, in cm.s^{-1})

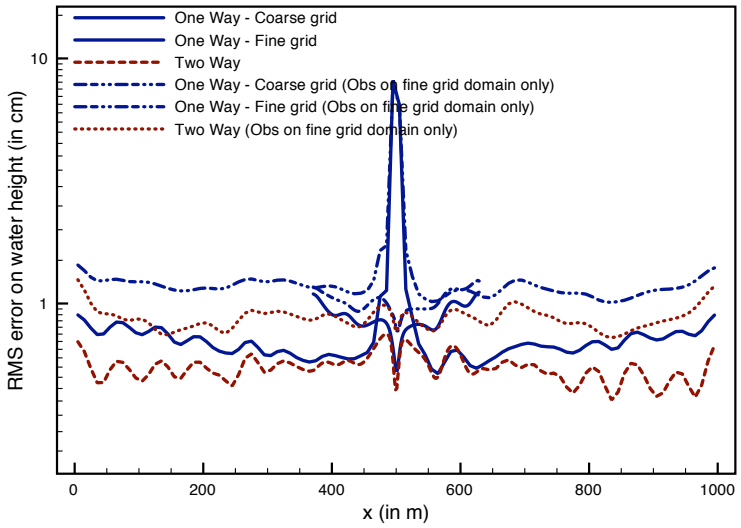

Figure 12: RMS errors (in logarithmic scale) for water height when observations are located either on the whole domain (three first curves) or on the fine grid domain only (three last curves). The fine grid domain is between x=370m and x=630m

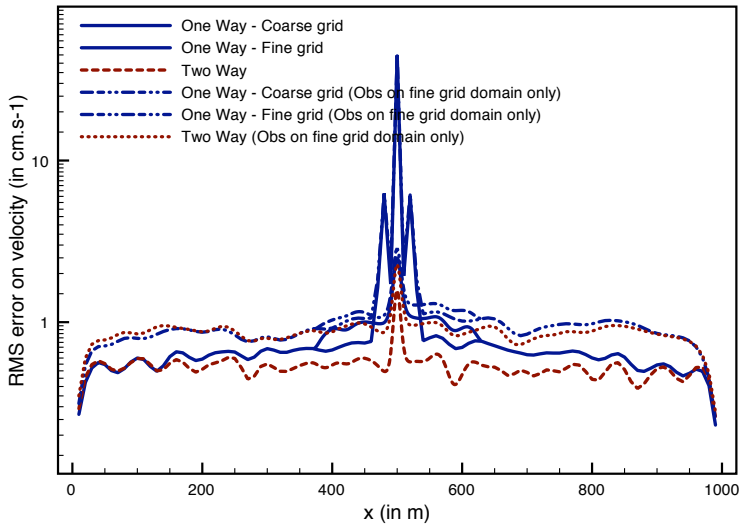

Figure 13: RMS errors (in logarithmic scale) for velocity when observations are located either on the whole domain (three first curves) or on the fine grid domain only (three last curves). The fine grid domain is between x=370m and x=630m